DELPHI Collaboration

DELPHI 2006-003 CONF 749
23 June, 2006

Search for single top quark production via contact interactions at LEP2

S. Andringa[1], N. Castro[1], M. Espírito-Santo[1], P. Gonçalves[1], O. Oliveira[2], A. Onofre[1,3], M. Pimenta[1], B. Tomé[1] and F. Veloso[1]

[1]LIP-IST-FCUL, Av. Elias Garcia, 14, 1, 1100-149 Lisboa, Portugal
[2]Dep. Física, Universidade de Coimbra, P-3004-516 Coimbra, Portugal
[3]UCP, R. Dr. Mendes Pinheiro, 24, 3080 Figueira da Foz, Portugal

Abstract

Single top quark production via four-fermion contact interactions associated to flavour-changing neutral currents was searched for in data taken by the DELPHI detector at LEP2. The data were accumulated at centre-of-mass energies ranging from 189 to 209 GeV, with an integrated luminosity of 598.1 pb^{-1}. No evidence for a signal was found. Limits on the energy scale Λ, were set for scalar-, vector- and tensor-like coupling scenarios.

Contributed Paper for ICHEP 2006 (Moscow)

1   Introduction

With a mass of 172.7 ± 2.9 GeV[1], the t quark is the heaviest known one and, due to its large mass, the most sensitive to new physics. In e^+e^- collisions at LEP2, t quarks could only be singly produced, due to the limited centre-of-mass energy. In the Standard Model (SM) they would be generated in association with b or c quarks, through the processes[1] $e^+e^- \to t\bar{b}e^-\bar{\nu}_e$ and $e^+e^- \to t\bar{c}$. A complete tree level calculation has shown that the cross-section of the first process is at the level of 10^{-6} pb [2]. The second process proceeds via Flavour Changing Neutral Currents (FCNC), which are forbidden at tree level and suppressed by the GIM mechanism [3] at higher orders. The corresponding cross-section is of the order of 10^{-12} pb [4].

Enhanced $e^+e^- \to t\bar{c}$ cross-sections (or top FCNC branching ratios) are, however, foreseen in several new physics scenarios, such as models with extra $Q = 2/3$ quark singlets [5], two Higgs doublet models (2HDM) [6, 7], flavour conserving 2HDM [7, 8], minimal supersymmetric SM [9, 10, 11] or non-minimal supersymmetric models with R parity violation [12]. Single t quark production at LEP2 would thus be a signature of new physics.

The four LEP collaborations [13, 14, 15, 16] searched previously for single t production in the context of Ref. [17]. In the model used, single t production is described in terms of vector-like anomalous couplings (κ_Z and κ_γ) associated with the already known Z and γ bosons. The physics energy scale was set to the t mass.

In this paper, a very general approach describing single t quark production via $e^+e^- \to t\bar{c}$ through an effective Lagrangian with FCNC operators is used. Apart from the Z and γ bosons, new four-fermion contact interactions, which include additional scalar-, vector-, and tensor-like couplings, are possible. The contribution of the Z boson is also included, through a vector-like coupling which can be related to the anomalous coupling κ_Z. The physics energy scale is a free parameter in this model. The kinematic differences between different coupling assumptions are taken into account and a dedicated analysis is developed.

This paper is organized as follows: Single t quark production and decay is briefly discussed in section 2. In section 3 the data sets and the simulated samples are presented. The analysis is described in section 4 and the results are presented in section 5. In section 6, conclusions are drawn and the results are compared with previous LEP studies.

2   Single t quark production and decay

The process $e^+e^- \to t\bar{c}$ can be described by an effective Lagrangian with FCNC operators [18]. Fig. 1 shows the Feynman diagrams considered in this model. New contact interaction terms are associated to new scalar (S_{RR}), vector (V_{ij}, $i,j = L, R$) and tensor-like (T_{RR}) couplings of heavy fields, and a term describing a new Ztc vertex parametrized by vector (a_j^Z) couplings is introduced.

The differential cross-section, for $t\bar{c}$ production only, can be obtained from the Lagrangian given in Ref. [18] and is expressed in terms of the couplings and of a new physics

---

[1]Throughout this paper the charge conjugated processes are also included, unless explicitly stated otherwise.

Scenarios	S_{RR}	V_{RR}	V_{RL}	V_{LR}	V_{LL}	T_{RR}	a_R^Z	a_L^Z
SVT	1	1	1	1	1	1	0	0
S	1	0	0	0	0	0	0	0
V	0	1	1	1	1	0	0	0
T	0	0	0	0	0	1	0	0
a	0	0	0	0	0	0	1	1
$V-a$	0	1	1	1	1	0	-1	-1
$V+a$	0	1	1	1	1	0	1	1

Table 1: The couplings used in the different scenarios considered in this paper.

energy scale parameter Λ:

$$
\frac{\mathrm{d}\sigma}{\mathrm{d}\cos\theta}(\mathrm{e}^+\mathrm{e}^- \to \mathrm{t\bar{c}}) = \frac{3\mathcal{C}}{8}\Bigg\{ S_{RR}^2(1+\beta) - 4S_{RR}T_{RR}(1+\beta)\cos\theta
$$

$$
+16T_{RR}^2\left(1 - \beta + 2\beta\cos^2\theta\right)
$$

$$
+2\left[\left(V_{RR} + 4c_R^Z a_R^Z \frac{m_W m_Z}{s - m_Z^2}\right)^2 + \left(V_{LL} + 4c_L^Z a_L^Z \frac{m_W m_Z}{s - m_Z^2}\right)^2\right]
$$

$$
\times\left[1 + (1+\beta)\cos\theta + \beta\cos^2\theta\right]
$$

$$
+2\left[\left(V_{RL} + 4c_R^Z a_L^Z \frac{m_W m_Z}{s - m_Z^2}\right)^2 + \left(V_{LR} + 4c_L^Z a_R^Z \frac{m_W m_Z}{s - m_Z^2}\right)^2\right]
$$

$$
\times\left[1 - (1+\beta)\cos\theta + \beta\cos^2\theta\right]\Bigg\}, \tag{1}
$$

where

$$
\mathcal{C} = \frac{s}{\Lambda^4}\frac{\beta^2}{4\pi(1+\beta)^3}, \quad \beta = \frac{(s - m_{\mathrm{t}}^2)}{(s + m_{\mathrm{t}}^2)}, \quad c_L^Z = -1/2 + \sin^2\theta_W, \quad c_R^Z = \sin^2\theta_W,
$$

β is the velocity of the outgoing t quark, θ_{W} is the electroweak mixing angle and θ is the angle between the incident electron beam and the t quark. The coupling scenarios listed in Table 1 were considered in this study. The "$V + a$" ("$V - a$") scenario corresponds to the constructive (destructive) interference between the eetc and the Ztc vertices. The differential cross-section depends on the coupling scenarios as can be seen in Fig. 2 for scenarios SVT, S, V and t, considering $m_{\mathrm{t}} = 175$ GeV/c^2, $\Lambda = 1$ TeV and $\sqrt{s} = 206$ GeV.

The total production cross-section, including charge conjugation, obtained from Equ. 1 is

$$
\sigma(\mathrm{e}^+\mathrm{e}^- \to \mathrm{t\bar{c}}) + \sigma(\mathrm{e}^+\mathrm{e}^- \to \mathrm{\bar{t}c}) = \mathcal{C}\Bigg\{ 8(3-\beta)T_{RR}^2 + \frac{3}{2}(1+\beta)S_{RR}^2 + (3+\beta) \times
$$

$$
\left[\left(V_{RR} + 4c_R^Z a_R^Z \frac{m_W m_Z}{s - m_Z^2}\right)^2 + \left(V_{LL} + 4c_L^Z a_L^Z \frac{m_W m_Z}{s - m_Z^2}\right)^2 + \right.
$$

$$
\left.\left(V_{RL} + 4c_R^Z a_L^Z \frac{m_W m_Z}{s - m_Z^2}\right)^2 + \left(V_{LR} + 4c_L^Z a_R^Z \frac{m_W m_Z}{s - m_Z^2}\right)^2\right]\Bigg\}. \tag{2}
$$

2

The total cross-section as a function of the centre-of-mass energy for $\Lambda = 1$ TeV is represented in Fig. 3. It can be seen that, for the scenarios mentioned above, the contribution from the Ztc vertex is about two orders of magnitude smaller than the one from the eetc vertex.

The Ztc vertex was described within other models by an anomalous coupling, κ_Z, as discussed in Ref. [17]. The couplings κ_Z and a_j^Z are related by:

$$\kappa_Z^2 = \left[\left(a_L^Z\right)^2 + \left(a_R^Z\right)^2\right]\left[2\cos\theta_W\left(\frac{v}{\Lambda}\right)^2\right]^2,$$ (3)

where $v = 246$ GeV is the SM Higgs vacuum expectation value.

The t quark is expected to decay mainly into Wb. The decays of the W into both quarks and leptons were considered, giving rise to a hadronic topology ($t\bar{c} \to b\bar{c}q\bar{q}'$) and a semi-leptonic topology ($t\bar{c} \to b\bar{c}\ell\bar{\nu}_\ell$).

3   Data samples and simulation

The data were collected with the DELPHI detector during the 1998, 1999 and 2000 LEP2 runs at $\sqrt{s} = 189 - 209$ GeV and correspond to a total integrated luminosity of 598.1 pb^{-1}. The integrated luminosity collected at each centre-of-mass energy is shown in Table 2.

DELPHI was constituted by several sub-detectors in cylindrical layers in the barrel region, which was closed by two endcaps that formed the forward region of the detector. The main sub-detectors used for the present analysis were the tracking detectors, the calorimeters and the muon chambers. Starting from the beam pipe, the barrel tracking detectors were a three layer silicon micro-vertex detector (the Vertex Detector), a combined drift/proportional chambers detector (the Inner Detector), the Time Projection Chamber (TPC) which was the main tracking detector and, finally, a 5 layer drift tube detector (the Outer Detector). The forward region was covered by drift chambers (the Forward Chambers A and B). The electromagnetic calorimeters were a sampling calorimeter of lead and gas in the barrel zone, the High-Density Projection Chamber, and a lead-glass calorimeter with 4532 blocks in each endcap, the Forward Electromagnetic Calorimeter. The Hadron Calorimeter was a sampling iron/gas detector in both the barrel and forward regions and in which the iron was simultaneously used as the magnet yoke. The Muon Chambers were sets of drift chambers which formed the outer surface of the DELPHI detector and were crucial for identifying muons, essentially the only particles that reached these detectors. A detail description can be found in Ref. [19]. During the year 2000 data taking, an irreversible failure affected one sector of the TPC, corresponding to 1/12 of its acceptance. The data recorded under these conditions were analysed separately.

The relevant SM background processes were simulated at each centre-of-mass energy using several Monte Carlo generators. All the four-fermion final states (both neutral and charged currents) were generated with WPHACT [20], while the particular phase space regions of $e^+e^- \to e^+e^-f\bar{f}$ referred to as $\gamma\gamma$ were generated using PYTHIA 6.1 [21]. The $qq(\gamma)$ final state was generated with KK2F [22]. Processes giving mainly leptonic final states were also generated, namely Bhabha events with BHWIDE [23], $e^+e^- \to \mu^+\mu^-$ events with KK2F and $e^+e^- \to \tau^+\tau^-$ events with KORALZ [24]. The fragmentation and hadronisation of the final-state quarks was handled by PYTHIA 6.1.

year	1998	1999	1999	1999	1999	2000	2000	2000
$\langle\sqrt{s}\rangle$ (GeV)	188.6	191.6	195.5	199.5	201.6	204.8	206.6	206.3*
$\mathcal{L}$ (pb^{-1})	153.0	25.1	76.0	82.7	40.2	80.0	81.9	59.2

Table 2: Integrated luminosity collected with the DELPHI detector at each centre-of-mass energy. The data collected during the year 2000 with the TPC fully operational were split into two energy bins, below and above $\sqrt{s} = 206$ GeV, with $\langle\sqrt{s}\rangle = 204.8$ GeV and $\langle\sqrt{s}\rangle = 206.6$ GeV, respectively. The last column, marked by an asterisk, corresponds to data collected with a reduced TPC acceptance.

For each coupling scenario, signal samples were generated using a modified version of PYTHIA 5.7 [25], where the angular distribution for t quark production was introduced according to Equ. 1 and considering $m_{\mathrm{t}} = 175$ GeV/c^2. Initial and final state radiation (ISR and FSR) were taken into account. The final-state quarks fragmentation and hadronisation was handled by JETSET 7.408 [25].

The generated signal and background events were passed through the detailed simulation of the DELPHI detector [19] and then processed with the same reconstruction and analysis programs as the data.

4 Analysis description

The analysis consisted of a sequential selection used to identify the event topology and reduce SM background contamination, followed by a probabilistic analysis based on the construction of a discriminant variable. Excepting a common preselection, the hadronic ($t\bar{c} \rightarrow b\bar{c}q\bar{q}'$) and the semi-leptonic ($t\bar{c} \rightarrow b\bar{c}\ell\bar{\nu}_\ell$) topologies were considered separately in each step of the analysis.

4.1 Sequential selection

A common preselection was adopted for both topologies, followed by specific selection criteria.

Events were preselected requiring at least eight good charged-particles tracks and a visible energy greater than $0.2\sqrt{s}$, measured at polar angles[2] above 20°. Good charged-particles tracks were selected by requiring a momentum above 0.2 GeV/c with a relative error below 1, and impact parameters along the beam direction and in the transverse plane below 4 cm/$\sin\theta$ and 4 cm, respectively.

The identification of muons relied on the association of charged particles to signals in the muon chambers and in the hadronic calorimeter and was provided by standard DELPHI algorithms [19], which classified each identified muon as *very loose*, *loose*, *standard* or *tight*. The identification of electrons and photons was performed by combining information from the electromagnetic calorimeters and the tracking system. Radiation and interaction effects were taken into account by an angular clustering procedure around

---

[2]In the standard DELPHI coordinate system, the positive z axis is along the electron direction. The polar angle θ is defined with respect to the z axis. In this paper, polar angle ranges are always assumed to be symmetric with respect to $\theta = 90°$.

the main shower [26]. Electron and photon candidates were classified as *loose* or *tight* by the identification algorithms.

The search for isolated particles (charged leptons and photons) was done by constructing double cones centered in the direction of charged-particle tracks or neutral energy deposits. The latter ones were defined as calorimetric energy deposits above 0.5 GeV, not matched to charged-particles tracks and identified as photon candidates by the standard DELPHI algorithms [19, 26]. For charged leptons (photons), the average energy density in the region between the two cones, which had half-opening angles of 5° and 25° (5° and 15°), was required to be below 150 MeV/° (100 MeV/°), to ensure isolation. The energy of the isolated particle was then re-evaluated as the sum of the energies inside the inner cone and was required to be above 5 GeV. For well identified leptons or photons the above requirements were weakened. In this case only the external cone was used and its angle α was varied according to the energy of the lepton (photon) candidate, down to 2° for $P_\ell \geq 70$ GeV/c (3° for $P_\gamma \geq 90$ GeV/c), with the allowed energy inside the cone reduced by $\sin\alpha/\sin 25°$ ($\sin\alpha/\sin 15°$).

The topology of each event was defined according to the number of isolated charged leptons identified in the event: events with no isolated charged leptons were classified as hadronic while all the other events were classified as semi-leptonic. Following the fragmentation and hadronisation, final state quarks were identified as jets. In both topologies, a b jet identified using the combined b-tag described in Ref. [27], and a low momentum jet from the c quark were expected. The events of the hadronic (semi-leptonic) topology were forced into four (two) jets[3], using the Durham jet algorithm [28].

After this common preselection specific selection criteria were applied to both topologies.

Hadronic topology

The final state of the hadronic topology ($t\bar{c} \to b\bar{c}q\bar{q}'$) is characterized by the presence of four jets, two of them from the W hadronic decay, and no missing energy. The distributions of relevant variables after the common preselection are shown in Fig. 4. Due to the high multiplicity expected in this topology, the required minimum number of good charged-particles tracks was raised to 25. The events were required to have an effective centre-of-mass energy [29] $\sqrt{s'} \geq 0.7\sqrt{s}$ and a thrust below 0.9. Events were clustered into four jets and it was required that $-\ln(y_{4\to3}) \leq 6.5$, where $y_{n\to n-1}$ is the Durham resolution variable in the transition from n to $n-1$ jets. Assuming a four-jets final state, a kinematic fit imposing energy-momentum conservation was performed. Events with χ^2 lower than 10 were accepted.

In Table 3 the number of selected data events, the expected SM background and the signal efficiencies for the different centre-of-mass energies at the end of the sequential selection are shown.

Semi-leptonic topology

The final state for the semi-leptonic topology ($t\bar{c} \to b\bar{c}\ell\bar{\nu}_\ell$) is characterised by the presence of two jets, one isolated and energetic lepton and missing energy. The b jet is expected to be energetic, while the c jet has low momentum. Events with at least one isolated

---

[3]Isolated charged leptons and isolated photons were excluded in the jet clustering.

$\langle\sqrt{s}\rangle$ (GeV)	188.6	191.6	195.5	199.5	201.6	204.8	206.6	206.3*
Hadronic topology:								
data	1165	211	613	637	306	599	606	400
background	1216.1	197.0	589.5	637.7	299.6	610.6	612.7	444.1
	±14.4	±2.3	±6.6	±7.0	±3.3	±6.6	±6.5	±4.8
ε min. (%)	46.5	42.8	42.8	50.9	50.9	51.5	51.5	50.5
ε max. (%)	48.2	48.9	48.9	54.0	54.0	55.6	55.6	54.5
Semi-leptonic topology – e sample:								
data	259	37	140	151	80	166	137	106
background	290.8	46.0	142.8	157.1	75.9	155.2	158.2	109.6
	±5.2	±0.8	±2.5	±2.8	±1.3	±2.7	±2.8	±2.0
ε min. (%)	6.5	6.1	6.1	6.4	6.4	6.5	6.5	6.2
ε max. (%)	7.6	7.3	7.3	7.2	7.2	7.1	7.6	7.1
Semi-leptonic topology – μ sample:								
data	423	75	226	259	111	240	220	169
background	432.9	75.4	225.6	246.7	118.4	232.8	244.3	169.9
	±6.5	±1.1	±3.3	±3.6	±1.7	±3.3	±3.5	±2.5
ε min. (%)	10.6	10.5	10.5	10.3	10.3	10.7	10.5	9.9
ε max. (%)	11.5	11.6	11.6	11.4	11.4	11.1	11.5	10.8
Semi-leptonic topology – *no-id* sample:								
data	308	49	140	135	67	145	148	92
background	286.2	45.4	133.9	146.8	72.0	141.1	141.7	104.5
	±7.5	±1.2	±3.3	±3.6	±1.7	±3.3	±3.4	±2.5
ε min. (%)	2.7	2.6	2.6	2.8	2.8	2.9	3.3	2.7
ε max. (%)	3.5	3.4	3.4	3.3	3.3	3.3	3.6	3.4
Total:								
data	2155	372	1119	1118	564	1150	1111	767
background	2226.0	363.8	1091.8	1188.3	565.9	1139.7	1156.9	828.1
	±18.2	±2.9	±8.5	±9.1	±4.3	±8.5	±8.6	±6.3
ε min. (%)	67.5	62.3	62.3	71.3	71.3	72.7	72.6	69.8
ε max. (%)	69.3	69.8	69.8	75.0	75.0	76.7	77.5	73.6

Table 3: Number of selected data events, expected SM background and signal efficiencies, ϵ, (in percent and convoluted with the branching ratio of the W boson) after the sequential selection. The expected background numbers are shown with their statistical errors. The efficiencies were computed for the different coupling scenarios according to Table 1 and the extreme values were chosen. The statistical errors on the efficiency are smaller than 2.1% and 0.1% for the hadronic and semi-leptonic topologies, respectively.

6

charged lepton and at least six good charged-particles tracks with TPC information were accepted. The particles of the events, excluding the isolated leptons, were clustered into two jets using the Durham algorithm and the events were divided into three mutually exclusive samples according to the identified flavour of the most energetic lepton: events with a *tight* electron ("e sample"), events with a *standard* or *tight* muon ("μ sample") and events in which no unambiguous lepton was present ("*no-id* sample")[4].

In the e and *no-id* samples, photons converting in the tracking system were vetoed by requiring that the lepton had left a signal in at least two layers of the vertex detector. In these samples, contamination from Bhabha and $\gamma\gamma$ events was reduced by imposing that the lepton was above 25° in polar angle and had an isolation angle (in relation to jets, isolated photons and other isolated charged leptons) greater than 10°. Additionally, in the *no-id* sample, these backgrounds were further rejected by keeping only events with exactly one isolated lepton, with momentum above $0.075\sqrt{s}$ and an isolation angle of at least 20°. The distributions of relevant variables after the common preselection are shown in Fig. 5. The q$\bar{\text{q}}$ background contamination, in the e and *no-id* samples, was further reduced by requiring a missing momentum above 10 GeV/c pointing above 25° in polar angle.

Assuming a jj$\ell\nu$ final state and assigning the missing momentum to the undetected neutrino, a kinematic fit imposing energy-momentum conservation was applied in all three samples. Events with χ^2 lower than 10 were accepted.

In Table 3 the number of selected data events, the expected SM background and the signal efficiencies are shown at the end of the sequential selection.

4.2 Discriminant selection

After the sequential analysis, the main background consisted of W$^+$W$^-$ events, which are similar to the signal and have the same final state topology. A separation is possible, based on the different kinematic properties and on jet-flavour tagging techniques. Furthermore, the W and t quark mass constraints can be used to separate signal and background.

Hadronic topology

In order to identify the b and c jets and determine the kinematic properties of the t quark and of the W boson, several possible jet assignment schemes were studied:

1. the most energetic jet is assigned to the b quark and the least energetic one to the c quark;

2. the most energetic jet is assigned to the b quark and the jets that minimise $|m_{\text{jj}} - m_{\text{W}}|$, where m_{jj} is the invariant mass of two of the three remaining jets and $m_{\text{W}} = 80.4$ GeV/c^2, are assigned to the W boson;

3. the jet with the highest b-tag value is assigned to the b quark and the least energetic one of the remaining three to the c quark;

4. the jet with the highest b-tag value is assigned to the b quark and, from the three remaining, the jets that minimise $|m_{\text{jj}} - m_{\text{W}}|$ are assigned to the W boson.

---

[4]Notice that, according to these definitions, the e and μ samples also contain the tauonic events in which the τ decayed, respectively, into a e (if classified as *tight*) or a μ (if classified as *standard* or *tight*).

Scheme:	1	2	3	4
$\sqrt{s} = 189$ GeV:				
ε_b (%):	52.4	52.4	72.5	72.5
ε_c (%):	45.5	43.4	41.9	40.7
$\sqrt{s} = 206$ GeV:				
ε_b (%):	53.3	53.3	68.0	68.0
ε_c (%):	51.2	51.0	47.1	44.8

Table 4: Fraction of the correct assignments of jets to quarks for simulated signal events of the hadronic topology at $\sqrt{s} = 189$ GeV and $\sqrt{s} = 206$ GeV, using the four jet assignment schemes explained in the text.

The correct assignment of jets to quarks was studied with simulated signal samples at $\sqrt{s} = 189$ GeV and $\sqrt{s} = 206$ GeV. Correct assignment was defined based on the angle α_{qj} between the quark and jet direction, requiring $\cos\alpha_{\mathrm{qj}} \geq 0.9$. The results are presented in Table 4: higher efficiencies for the b quark assignment are obtained with schemes 3 and 4. Scheme 3 was adopted since it also yields the best discrimination between signal and background.

Signal and background-like probabilities were assigned to each event based on Probability Density Functions (PDF) constructed with the following variables:

- the event b-tag value, $C_{\mathrm{b\text{-}tag}}^{\mathrm{event}}$;

- the b momentum, P_{b};

- the W reconstructed mass, m_{W}.

The distributions of these variables are shown in Fig. 6 for data, expected background and signal at $\langle\sqrt{s}\rangle = 206.6$ GeV. For each of these variables, the corresponding PDF for the signal (P_S^i) and background (P_B^i) were estimated. For each event, a signal likelihood ($P_S = \prod_i P_S^i$) and background likelihood ($P_B = \prod_i P_B^i$) were computed assuming no correlations. The discriminant variable was defined as $\ln\mathcal{L}_R = \ln(P_S/P_B)$. The distributions of $\ln\mathcal{L}_R$ for data, simulated background and signal are shown in Fig. 8a for $\langle\sqrt{s}\rangle = 206.6$ GeV.

Semi-leptonic topology

A discriminant variable was constructed using signal (P_S^i) and background (P_B^i) PDFs estimated from the following variables:

- the angle between the two jets, $\alpha_{j_1 j_2}$;

- the angle between the lepton and the neutrino, $\alpha_{\ell\nu}$;

- the reconstructed mass of the two jets, $m_{j_1 j_2}$;

- the reconstructed mass of the jet with the highest b-tag, the lepton and the neutrino, $m_{\mathrm{b}\ell\nu}$;

- the reconstructed W mass, $m_{\ell\nu}$;

8

- the ratio of the jet momenta, P_{j_2}/P_{j_1};

- the b-tag of the most energetic jet, $C_{\text{b-tag}}^{j_1}$;

- the product of the lepton charge and the cosine of the lepton polar angle, $Q_\ell \times \cos\theta_\ell$;

- $-\ln y_{2\to 1}$, where $y_{2\to 1}$ is the Durham resolution variable in the transition from two to one jet.

Distributions of some of these variables are shown in Fig. 7 for $\langle\sqrt{s}\rangle = 206.6$ GeV. The distributions of the discriminant variables $\ln\mathcal{L}_R = \ln(\prod_i P_S^i / \prod_i P_B^i)$ obtained at $\langle\sqrt{s}\rangle = 206.6$ GeV are shown in Fig. 8b–d for data, expected background and signal.

5 Results

The discriminant variables obtained in the different search channels are shown in Fig. 8, for $\langle\sqrt{s}\rangle = 206.6$ GeV. As no signal was found in any of the analysis channels, limits at 95% confidence level (CL) on the energy scale Λ were derived for each of the scenarios in Table 1. The limits were obtained using the modified frequentist likelihood ratio method [30], taking into account the observed and expected event counts, the signal efficiencies and the shapes of the discriminant variables in data, background and signal. The expected limit was computed as the median limit for experiments without signal contributions. The $\pm 1\sigma$ values around the expected median limit were also computed. In order to avoid non-physical fluctuations in the distributions of the discriminant variables, due to the limited statistics of the generated events, a smoothing procedure was adopted. The limits were evaluated assuming $m_{\text{t}} = 175$ GeV/c^2, which allows direct comparison with other published results. The results, obtained with the contribution of all the systematic uncertainties described in the next paragraph, are presented in Table 5. The observed and expected limits are statistically compatible and the maximum difference is about 1σ. The effect of a change in the t mass was studied at two extreme energies (188.6 and 204.8 GeV) and two extreme scenarios (SVT and a), considering the values 170 and 180 GeV/c^2 for m_{t}. The estimated relative changes in the limits were about $+10\%$ for $m_{\text{t}} = 170$ GeV/c^2 and -14% for $m_{\text{t}} = 180$ GeV/c^2. For scenarios S and T, in which only one coupling is non-zero, limits at 95% CL on the ratio between the coupling and Λ^2 can be directly obtained from Equ. 2:

$$\left(\frac{T}{\Lambda^2}\right)_{\text{obs}} \leq 6.90 \times 10^{-7} \text{GeV}^{-2}, \quad \left(\frac{T}{\Lambda^2}\right)_{\text{exp}} \leq 6.88 \times 10^{-7} \text{GeV}^{-2},$$

$$\left(\frac{S}{\Lambda^2}\right)_{\text{obs}} \leq 2.14 \times 10^{-6} \text{GeV}^{-2}, \quad \left(\frac{S}{\Lambda^2}\right)_{\text{exp}} \leq 2.43 \times 10^{-6} \text{GeV}^{-2}.$$

The limit obtained in scenario a, involving only the a_j^Z couplings, can be converted into a limit on the anomalous coupling κ_{Z} (see Equ. 3)[5], yielding $\kappa_{\text{Z}}^{\text{obs}} \leq 0.42$.

The evaluation of the limits was performed taking into account systematic uncertainties, which affect the background estimation and the signal efficiency. The stability of the sequential analysis was studied by changing the cut values in the most relevant variables

---

[5]Notice that in Ref. [13, 14, 15, 16] the contribution from the processes $e^+e^- \to t\bar{u}$ and $e^+e^- \to \bar{t}u$ are also considered. This was taken into account in the limits conversion.

Scenario	Hadronic topology				Semi-leptonic topology				Combined topologies			
	obs.	-1σ	exp.	$+1\sigma$	obs.	-1σ	exp.	$+1\sigma$	obs.	-1σ	exp.	$+1\sigma$
SVT	1225	1269	1188	1104	1318	1405	1311	1203	1404	1481	1376	1271
S	582	601	562	521	653	652	607	557	684	690	642	593
V	952	1002	933	866	998	1075	997	919	1074	1145	1068	984
T	1073	1128	1047	975	1124	1232	1144	1053	1204	1292	1206	1119
a	438	462	431	403	472	512	475	436	500	539	499	461
$V-a$	966	1017	945	877	1020	1100	1022	940	1094	1165	1084	1002
$V+a$	939	981	917	848	988	1082	1003	921	1062	1130	1058	977

Table 5: Observed and expected 95% CL lower limits on Λ (GeV) for the different scenarios, assuming $m_{\mathrm{t}} = 175$ GeV/c^2. The $\pm 1\sigma$ values around the expected median limit are also shown.

by typically 10%. The maximum relative change in the limit was about 2%. Different parameterisations inside PYTHIA were used to study the dependence of the efficiency on the hadronisation and fragmentation of the jets associated to heavy quarks. The Lund symmetric fragmentation, the Bowler space-time picture of string evolution and the Peterson/SLAC function were considered[6]. The maximum relative change in the limit was about 2%. The effect of PDF binning and smoothing procedures was studied and the maximum relative change in the limit was about 3%. A similar study was performed for the discriminant variables and the maximum relative change in the limit was about 6%.

6 Conclusions

Single top quark production via contact interactions was searched for using data collected by the DELPHI detector at centre-of-mass energies ranging from 189 GeV to 209 GeV, corresponding to an integrated luminosity of 598.1 pb^{-1}. The coupling scenarios listed in Table 1 were considered and a dedicated analysis was developed. No evidence for a signal was found. Limits at 95% confidence level on the new physics energy scale Λ were obtained and the observed values for different scenarios range from 500 GeV to 1404 GeV (see Table 5). The observed limit on the anomalous coupling κ_{Z}, obtained from the conversion of scenario a limit, is $\kappa_{\mathrm{Z}}^{\mathrm{obs}} \leq 0.42$.

The L3 collaboration also searched for single t quark production via contact interactions and the results agree with those presented here [13]. The converted limit on the anomalous coupling κ_{Z} agrees with those presented by the four LEP collaborations [13, 14, 15, 16] in the framework of Ref. [17].

Acknowledgements

---

[6]See [25] for more details.

References

[1] CDF Collaboration, D0 Collaboration and Tevatron Electroweak Working Group, *Combination of CDF and DØ results on the top-quark mass*, prepared for EPS-HEP 2005. [hep-ex/0507091].

[2] E. Boos *et al.*, *Phys. Lett.* **B326** (1994) 190.

[3] S. L. Glashow, J. Iliopoulos and L. Maiani, *Phys. Rev.* **D2** (1970) 1285.

[4] C. S. Huang, X. H. Wu and S. H. Zhu, *Phys. Lett.* **B452** (1999) 143.

[5] J. A. Aguilar-Saavedra, *Phys. Rev.* **D67** (2003) 035003;
Erratum-ibid. *Phys. Rev.* **D69** (2004) 099901.

[6] D. Atwood, L. Reina and A. Soni, *Phys. Rev.* **D53** (1996) 1199.

[7] D. Atwood, L. Reina and A. Soni, *Phys. Rev.* **D55** (1997) 3156.

[8] S. Bejar, J. Guasch and J. Sola, *Nucl. Phys.* **B600** (2001) 21.

[9] J. J. Liu, C. S. Li, L. L. Yang and L. G. Jin, *Phys. Lett.* **B599** (2004) 92.

[10] D. Delepine and S. Khalil, *Phys. Lett.* **B599** (2004) 62.

[11] J. Guasch and J. Sola, *Nucl. Phys.* **B562** (1999) 3.

[12] J. M. Yang, B. L. Young and X. Zhang, *Phys. Rev.* **D58** (1998) 055001.

[13] L3 Coll., P. Achard *et al.*, *Phys. Lett.* **B549** (2002) 290.

[14] ALEPH Coll., R. Barate *et al.*, *Phys. Lett.* **B494** (2000) 33;
ALEPH Coll., A. Heister *et al.*, *Phys. Lett.* **B543** (2002) 173.

[15] DELPHI Coll., J. Abdallah *et al.*, *Phys. Lett.* **B590** (2004) 21.

[16] OPAL Coll., G. Abbiendi *et al.*, *Phys. Lett.* **B521** (2001) 181.

[17] V. F. Obraztsov, S. R. Slabospitsky and O. P. Yushchenko, *Phys. Lett.* **B426** (1998) 393.

[18] S. Bar-Shalom and J. Wudka, *Phys. Rev.* **D60** (1999) 094016.

[19] DELPHI Coll., P. Aarnio *et al.*, *Nucl. Instrum. Methods* **A303** (1991) 233;
DELPHI Coll., P. Abreu *et al.*, *Nucl. Instrum. Methods* **A378** (1996) 57.

[20] E. Accomando and A. Ballestero, *Comp. Phys. Comm.* **99** (1997) 270;
E. Accomando *et al.*, *Comp. Phys. Comm.* **150** (2003) 166;
A. Ballestrero *et al.*, *Comp. Phys. Comm.* **152** (2003) 175.

[21] T. Sjöstrand *et al.*, *Comp. Phys. Comm.* **135** (2001) 238.

[22] S. Jadach, B.F.L. Ward and Z. Was, *Comp. Phys. Comm.* **130** (2000) 260.

[23] S. Jadach, W. Płaczek and B.F.L. Ward, *Phys. Lett.* **B390** (1997) 298.

[24] S. Jadach, B.F.L. Ward and Z. Was, *Comp. Phys. Comm.* **79** (1994) 503.

[25] T. Sjöstrand, *Comp. Phys. Comm.* **82** (1994) 74;
T. Sjöstrand, *PYTHIA 5.7 and JETSET 7.4*, CERN-TH/7112-93.

[26] F. Cossutti *et al.*, *REMCLU: a package for the Reconstruction of ElectroMagnetic CLUsters at LEP200*, DELPHI Note 2000-164 PROG 242.

[27] DELPHI Coll., J. Abdallah *et al.*, *Eur. Phys. J.* **C32** (2004) 185.

[28] S. Catani *et al.*, *Phys. Lett.* **B269** (1991) 432.

[29] P. Abreu *et al.*, *Nucl. Instrum. Methods* **A427** (1999) 487.

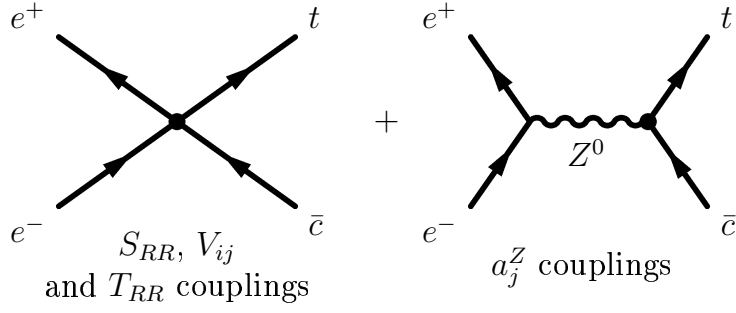[30] A. L. Read, CERN report 2000-005 (2000) 81.

Figure 1: The eetc and Ztc vertex contributions to the $e^+e^- \rightarrow t\bar{c}$ process.
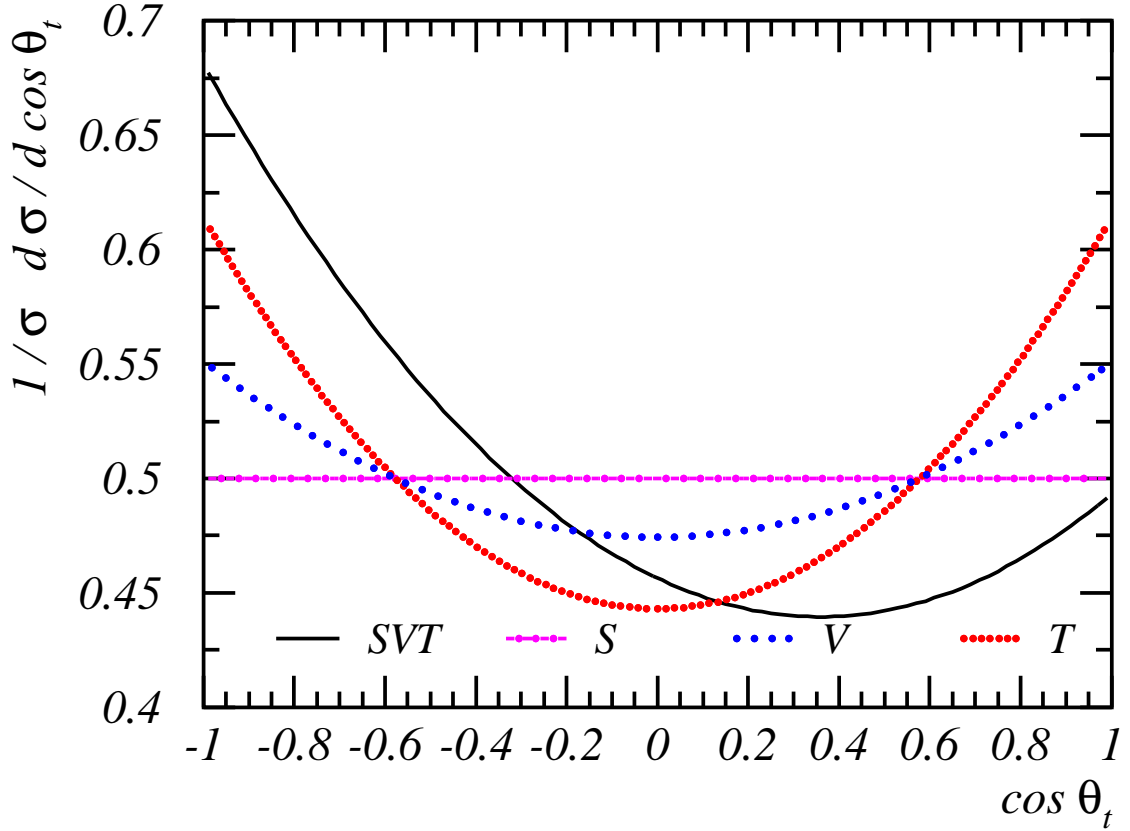

Figure 2: The differential cross-section $d\sigma/d\cos\theta_t$, normalized to the total cross-section, for the process $e^+e^- \rightarrow t\bar{c}$ without ISR is shown as a function of the cosine of the polar angle of the t quark, for $m_t = 175$ GeV/c^2, $\Lambda = 1$ TeV, $\sqrt{s} = 206$ GeV and the scenarios described in Table 1. The differential cross-sections for scenarios a, $V-a$ and $V+a$ are the same as scenario V.
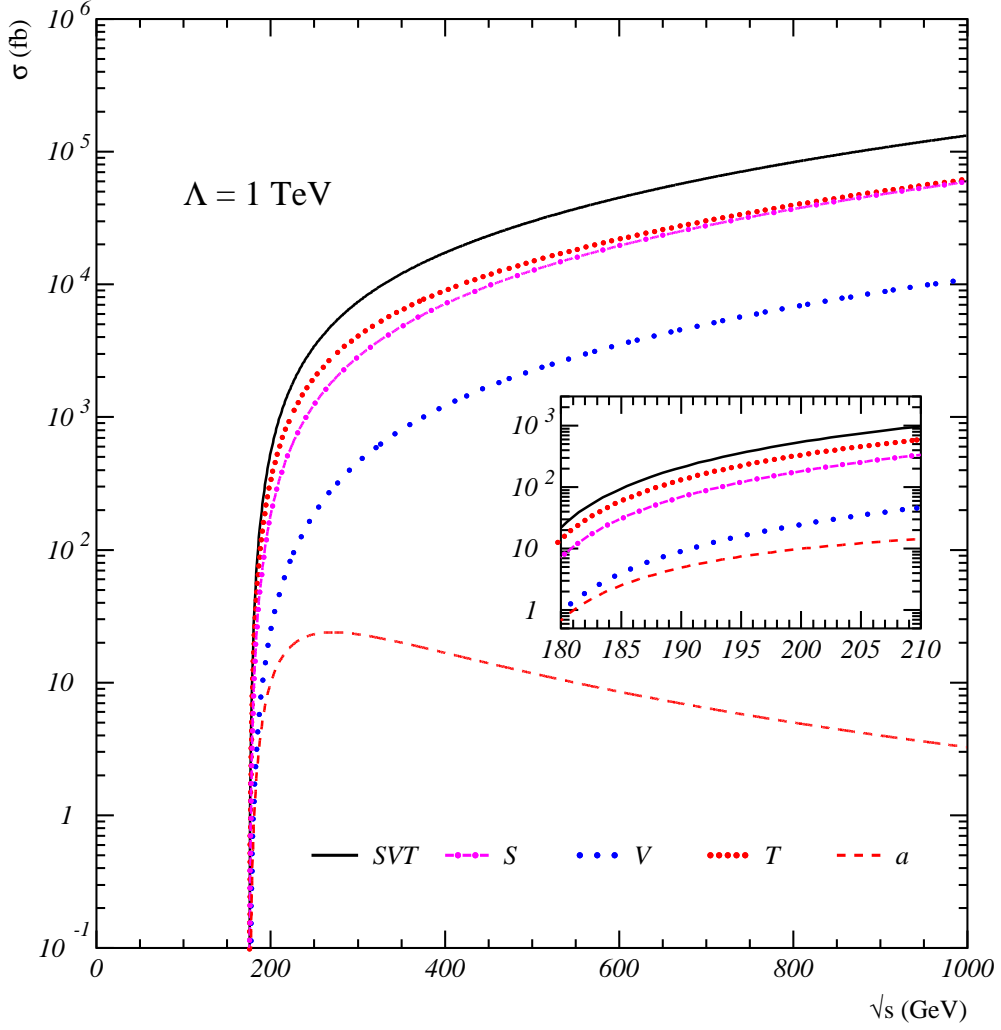
Figure 3: The total cross-section $\sigma_{\text{tc}} = \sigma(e^+e^- \to t\bar{c} + \bar{t}c)$ is shown as a function of the centre-of-mass energy, for $m_{\text{t}} = 175 \text{ GeV}/c^2$, $\Lambda = 1$ TeV and for the scenarios described in Table 1. In this scale the cross-sections for scenarios $V - a$ and $V + a$ are indistinguishable from the cross-section for scenario V. The inner box is a zoomed version of the plot in the $180 - 210$ GeV region.
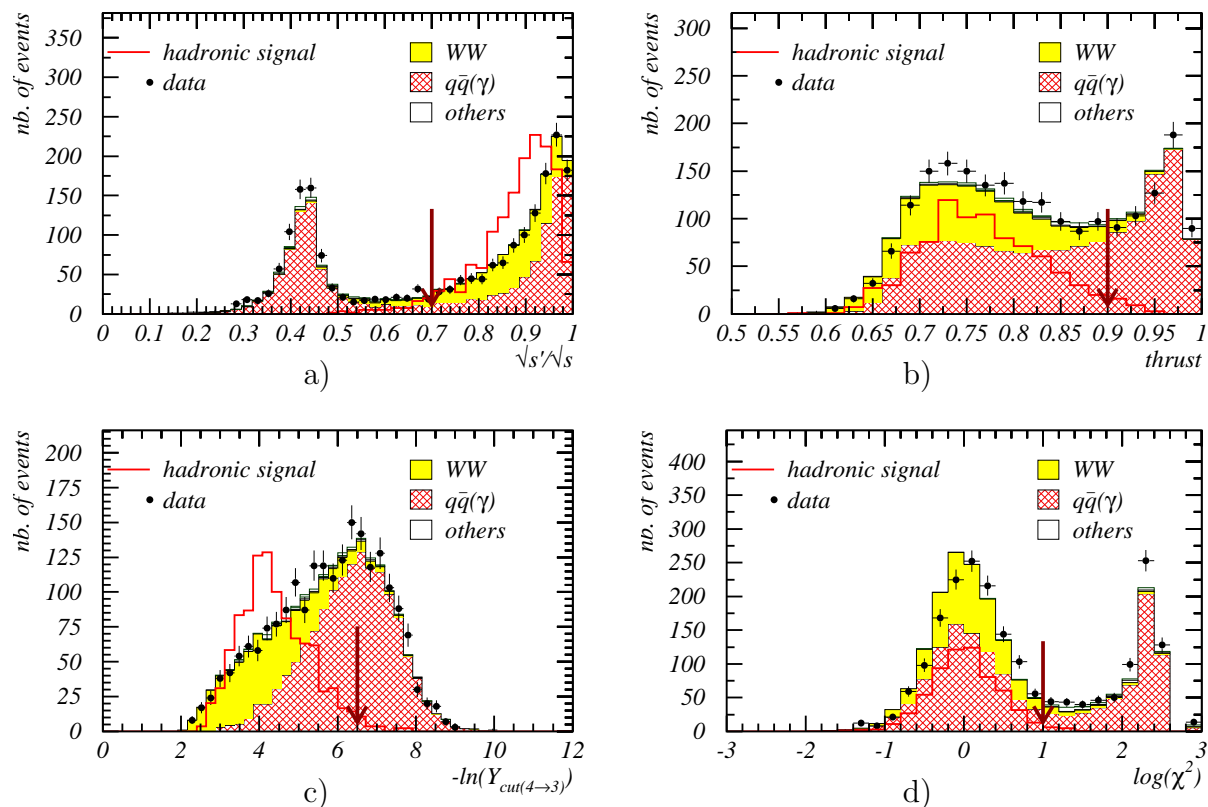
Figure 4: Distributions of variables relevant for the sequential selection of the hadronic topology are shown at $\langle\sqrt{s}\rangle = 206.6$ GeV: a) ratio between the effective centre-of-mass energy and the centre-of-mass energy; b) thrust; c) $-\ln(y_{4\to3})$; d) χ^2 of the kinematic fit imposing energy-momentum conservation. The WW, q$\bar{\text{q}}(\gamma)$ and "others" labels represent the background contribution from charged-current four-fermion final states generated with WPHACT [20], two fermion final states generated with KK2F [22] and all the other processes mentioned in section 3, respectively. The signal normalisation is arbitrary. The arrows show the applied cuts.
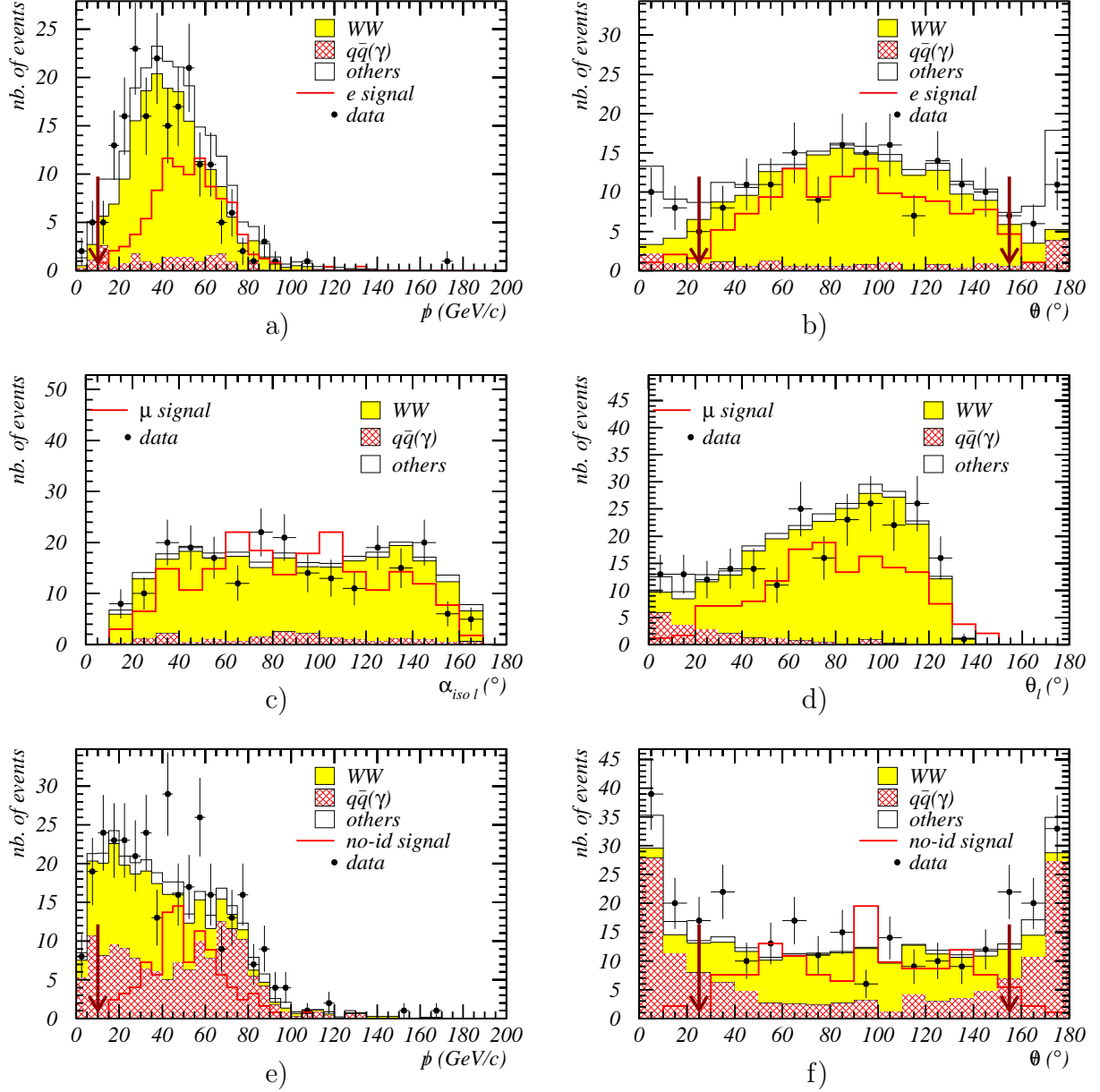
DELPHI

Figure 5: Distributions of variables relevant for the sequential selection of the semi-leptonic topology are shown at $\langle\sqrt{s}\rangle = 206.6$ GeV. e sample: a) missing momentum; b) polar angle of the missing momentum; μ sample: c) lepton polar angle; d) lepton isolation angle; *no-id* sample: e) missing momentum; f) polar angle of the missing momentum; The WW, q$\bar{q}(\gamma)$ and "others" labels have the same meaning as in Fig. 4. The signal normalisation is arbitrary. The arrows show the applied cuts.
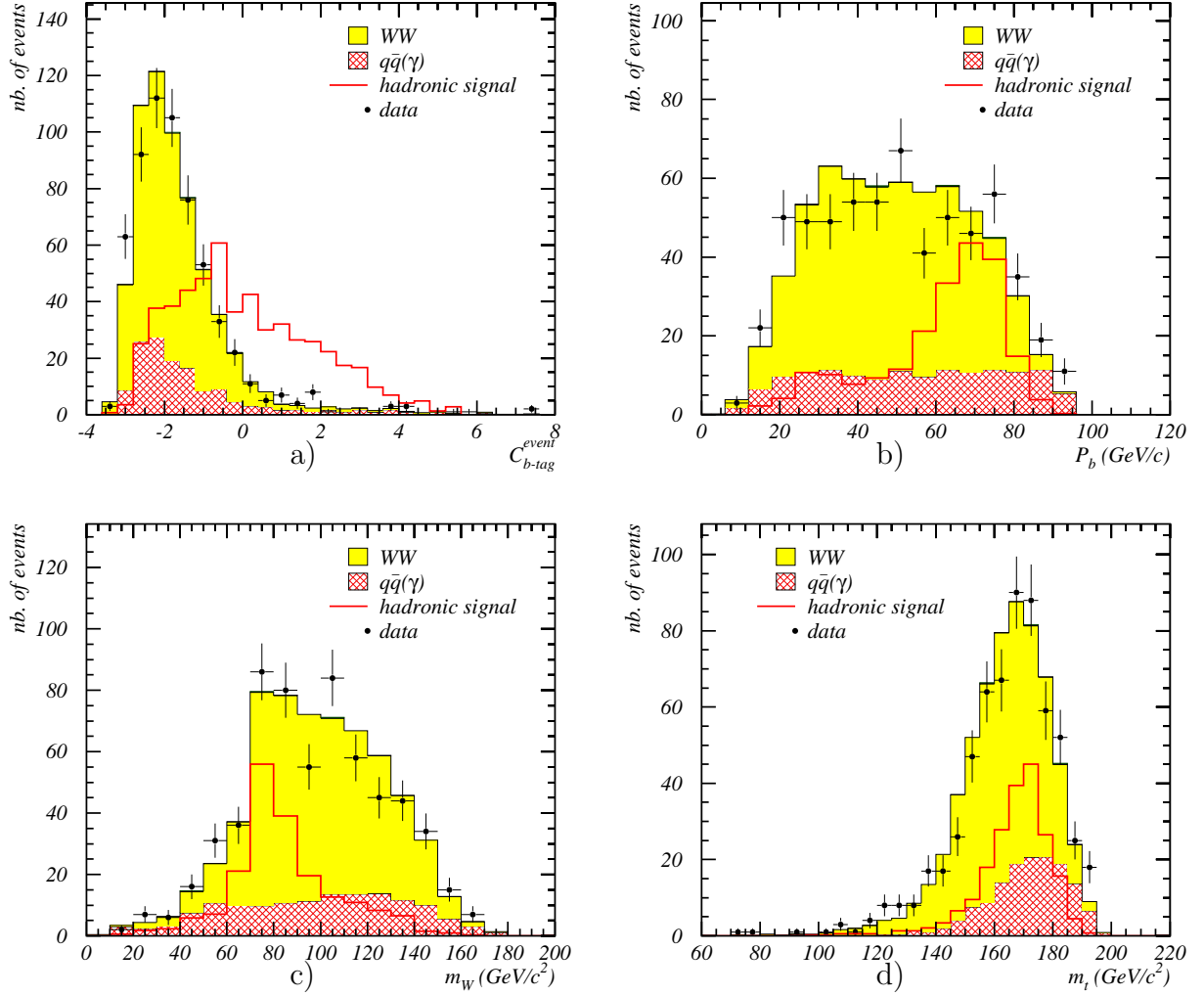
DELPHI

Figure 6: Distributions of variables relevant for the hadronic topology after the sequential selection at $\langle\sqrt{s}\rangle = 206.6$ GeV: a) b-tag of the event; b) b jet momentum; c) reconstructed W boson mass; d) reconstructed t quark mass. The a), b) and c) distributions were used as PDF to construct the discriminant variable for the the hadronic topology. The signal normalisation is arbitrary.
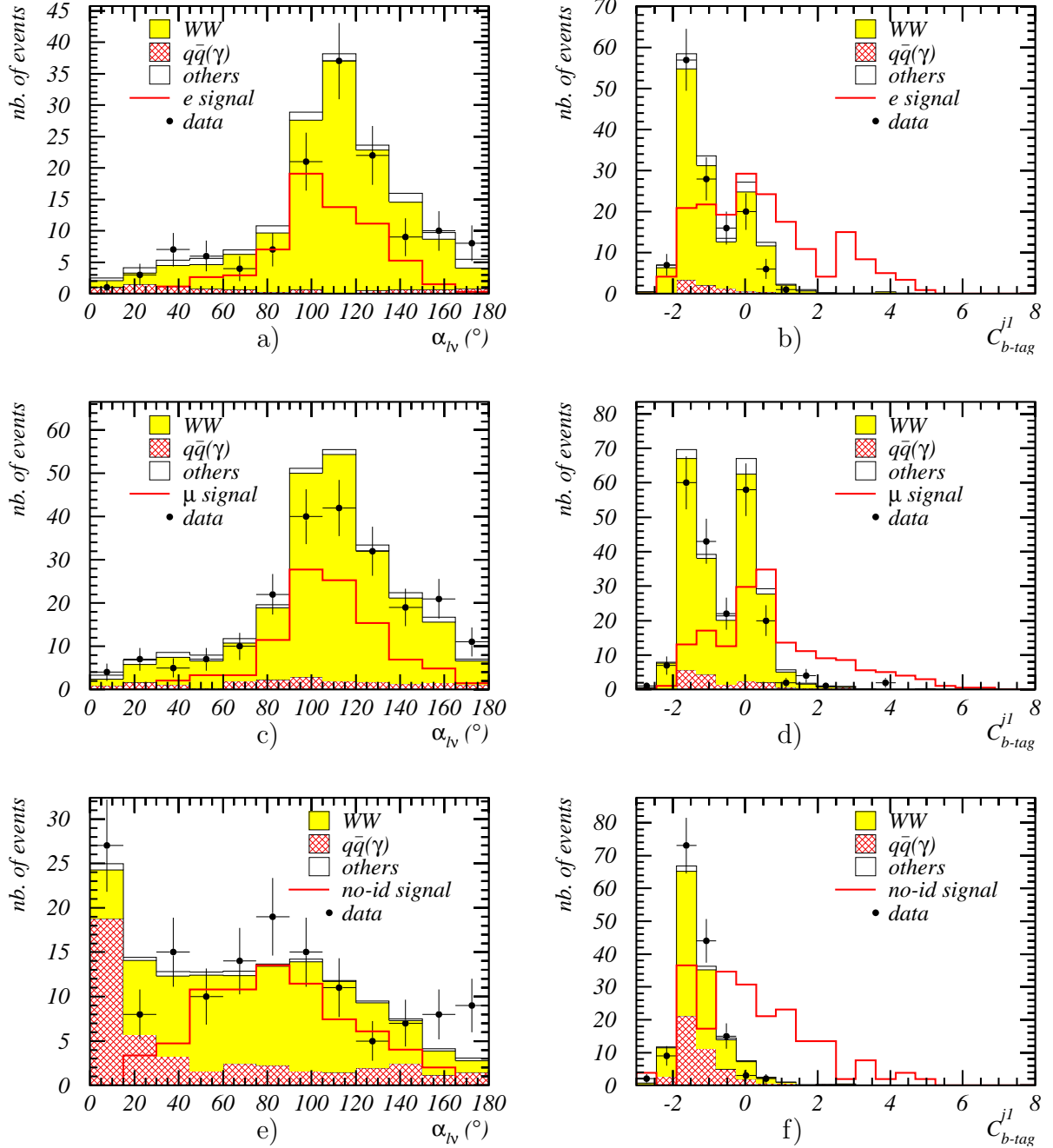
DELPHI

Figure 7: Distributions of variables relevant for the semi-leptonic topology after the sequential selection at $\langle\sqrt{s}\rangle = 206.6$ GeV In the left column: angle between the lepton and the neutrino; in the right column: b-tag of most energetic jet; (a,b) e sample; (c,d) μ sample; (e,f) *no-id* sample. The signal normalisation is arbitrary.
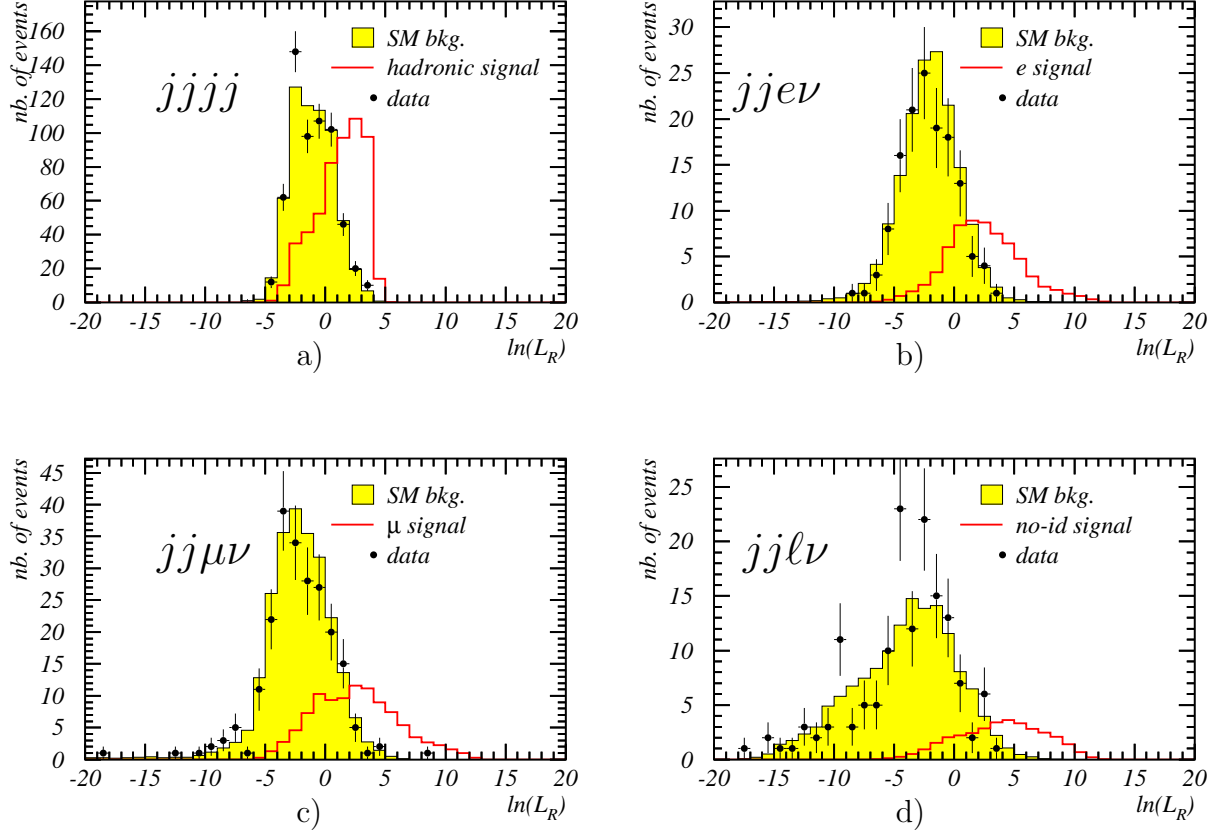
18

DELPHI

Figure 8: Distributions of the discriminant variable $\ln\mathcal{L}_R$ for data, expected background and signal after the sequential selection at $\langle\sqrt{s}\rangle$ = 206.6 GeV: a) hadronic topology; semi-leptonic topology: b) e sample; c) μ sample; d) *no-id* sample. These distributions correspond to scenario a (see Table 1). For the other scenarios, the discriminant variables do not change significantly. The signal normalisation is arbitrary, but the same in all plots.